Korea-Australia Rheology Journal, 31(3), 149-166 (August 2019) www.springer.com/13367
DOI: 10.1007/s13367-019-0016-3

Predicting the excess pressure drop incurred by LPTT fluids in flow through a planar constricted channel

Taha Rezaee[1], Mostafa Esmaeili[2], Solmaz Bazargan[3] and Kayvan Sadeghy[1,*]
[1]*School of Mechanical Engineering, College of Engineering, University of Tehran, Tehran 11155-4563, Iran*
[2]*Department of Mechanical Engineering, Faculty of Engineering, Kharazmi University, Tehran 15719-14911, Iran*
[3]*Satellite Research Institute, Iranian Space Research Center, Tehran 1997994313, Iran*

(Received February 11, 2019; final revision received June 29, 2019; accepted July 6, 2019)

Laminar flow of a viscoelastic fluid obeying the linear simplified Phan-Thien/Tanner model (LPTT) is numerically studied in a planar channel partially obstructed by a cosinusoidal constriction. Based on published data (Tammadon-Jahromi *et al*., 2011) there is no excess pressure drop for this particular fluid when flowing through an orifice-plate. Numerical results obtained using OpenFoam software at a typically low Reynolds number suggest that there exists a strong competition between the fluid's strain-hardening/shear-thinning behavior on the one side with its first normal-stress difference in extension, on the other side, in controlling the pressure drop caused by the presence of the constriction. It is shown that, an excess-pressure-drop (*epd*) can correctly be predicted provided that use is made of a proper (inelastic) baseline in the definition of the "*epd*". At moderate Reynolds numbers a flow-reversal is predicted to occur at the lee side of the constriction ruling out this technique as an extensional rheometer. It is argued that such vortices can be very useful in high-throughput microfluidic systems for mixing enhancement. To reduce the excessive pressure drop experienced by the fluid when working at high Reynolds numbers, it is shown that the Deborah number of the flow should be increased.

Keywords: Phan-Thien/Tanner model, constricted channel, Deborah number, extensional viscosity, OpenFoam, retardation parameter

1. Introduction

The flows of viscous fluids through constricted channels are frequently encountered in physiological systems and certain industrial applications. While in physiological systems they are troublesome in the sense that they can generate regions of excessive shear (Anderson *et al.*, 2000), in polymer industry the pressure drop incurred this way turns out to be useful for the measurement of the fluid's extensional viscosity (James *et al.*, 1990; Wang and James, 2011). The latter application works on the idea that for viscoelastic fluids there exists a large excess pressure drop (*epd*) in comparison with its Newtonian counterpart. In fact, for highly elastic fluids called Boger fluids, the experimental *epd* obtained in an axisymmetric channel (Perez-Camacho *et al.*, 2015) has been shown to correlate well with the extensional viscosity data (Lopez-Aguilar *et al.*, 2017). With the viscosity of Boger fluids being (nearly) constant (James, 2009), the excess pressure drop is rightly attributed to the fluid's elasticity, as manifested by its first normal-stress-difference in extension. In planar channels, the *epd* has been realized to be smaller than the axisymmetric channels (Aguayo *et al.*, 2008; Tammadon-Jahromi *et al.*, 2016). Nevertheless, it is still very attractive simply because "microfluidic extensional rheometers" appear to be the future of extensional rheometry (Rodd *et al.*, 2005; Rodd *et al.*, 2010; Wang and James, 2011; Sousa *et al.* 2011, Ober *et al.*, 2013; Lee and Muller, 2017).

Thanks to its application in extensional rheometry, extensive efforts were made in the past to predict the *epd* using viscoelastic fluids models such as Oldroyd-B. Here we briefly review the knowledge gathered over the years in this area. The focus would be on planar channels as noted above. One can particularly mention the creeping-flow numerical results obtained by Binding *et al.* (2006) in a planar channel equipped with a rounded-corner orifice-plate. They showed that depending on the Deborah number and the solute viscosity ratio, the Oldroyd-B model (commonly used to represent Boger fluids) may fail to predict *epd*. In an ensuing work, Walters *et al.* (2009) argued that the failure of this fluid model in predicting *epd* can be attributed to its excessive (quadratic) first normal-stress-difference (N1) which eclipses the favorable effect of the fluid's extensional viscosity in producing an excess pressure drop. The favourable role played by the extensional viscosity on *epd* has been beautifully demonstrated by Nyström *et al.* (2016). They resorted to the White-Metzner variation of the FENE-CR model called WM-FENE-CR (White and Metzner, 1963) and showed that for this particular constant-viscosity viscoelastic fluid model an excess pressure drop can indeed be predicted in creep-

*Corresponding author; E-mail: sadeghy@ut.ac.ir

ing flow through a constricted channel (This fluid model exhibits a much stronger strain-hardening behavior as compared with the FENE-CR model while their N1 behavior is virtually the same). Their success in predicting *epd* suggests that for the excess pressure drop to be predicted correctly for Boger fluids use should be made of rheological models for which the extensional viscosity is high but the first-normal-stress difference in shear is low. None of these rheological models can predict a non-zero second-normal-stress difference in shear (N2). In fact, Boger fluids are known to exhibit a negative N2 which is much smaller than N1 (Magda *et al.*, 1991).

To investigate the role played by N2 on the pressure drop in flow through constricted channels, Wapperom and Keunings (2000; 2001) resorted to two different viscoelastic fluid models, *i.e.*, the Pom-Pom model (Lee *et al.*, 2002), and the MGI model (Marrucci *et al.*, 2001). While for Pom-Pom model N2 is zero, for the MGI model it is non-zero and negative. Both models exhibit virtually the same viscous and N1 behavior in simple shear. Wapperom and Keunings (2000; 2001) showed that in creeping flow through a planar 4:1:4 constriction, both fluids experience virtually the same pressure drop, which was found to be a decreasing function of the Deborah number. Their results suggest that N2 plays no role on the pressure drop in planar constricted channels (For the axisymmetric version of such channels, however, it is easy to show that N2 plays an important role; see James *et al.* (1990)). They did not plot any *epd* results but from their pressure drop data it is obvious that for both fluid models, the *epd* is a decreasing function of the Deborah number. Since in extensional flows, the Pom-Pom model predicts a weak strain-hardening behavior followed by a weak strain-softening behavior whereas the MGI model is good only for strain-softening materials, these results again signify the importance of the extensional viscosity on the excess pressure drop. Moreover, by fitting the purely-viscous Carreau-Yasuda model to the viscosity data of the MGI model, Wapperom and Keunings (2000; 2001) showed that the pressure drop decreases by an increase in the degree of fluid's shear-thinning behavior.

To further explore the role played by shear-thinning, Tammadon-Jahromi *et al.* (2011) resorted to the Phan-Thien/Tanner model in their numerical study (Phan-Thien and Tanner, 1977). This fluid model is often regarded as one of the best rheological models when it comes to representing polymeric liquids (Peters *et al.*, 1999). In its most general form, a fluid obeying this model exhibits a strong shear-thinning behavior accompanied by a positive N1 which is non-quadratic and a negative N2 which is much smaller than N1. In extension, it can represent both strain-hardening and strain-softening materials depending on its parameter settings. In fact, there are variations of the model which can represent fluids showing a bounded value for the extensional viscosity and also fluids exhibiting a maximum in their extensional viscosity (Phan-Thien, 1978). In certain polymer processing operations such as extrusion, a knowledge about their extensional viscosity might be needed for design purposes. To that end, Tammadon-Jahromi *et al.* (2011) tried to investigate the applicability of *epd*-method for assessing the extensional viscosity of the linear form of this fluid model (LPTT). They resorted to a 4:1:4 contraction-expansion geometry - in the form of a rounded-corner orifice plate - but could not predict any excess pressure drop (see Figs. 14 and 15 in their work) inferring that perhaps this technique is not so viable for measuring the extensional viscosity of all viscoelastic fluids. They have concluded that perhaps the over-strong effect of shear-thinning is dominating over the effect of the first normal-stress-difference. No shear stress and/or first-normal-stress difference data were presented by them to support their conclusion (Actually, such data have been provided by them in simple shear flow, but data obtained in simple shear are of no consequence in constricted-channel flows where the rate of deformation is non-homogeneous in the constricted area).

The present work can be regarded as an extension of the work carried out by Tammadon-Jahromi *et al.* (2011) albeit admittedly the two geometries are not exactly the same. We show that for a Phan-Thien/Tanner fluid flowing through a constricted channel of cosinusoidal shape, an excess pressure drop can indeed be recorded as a function of the Deborah number provided that instead of the Newtonian baseline, *epd* is judged based on the fluid's inelastic analogue. To that end, a major part of our results has been devoted to low-Reynolds number flows (but without dropping the weak inertia terms). Still, thanks to the application of constricted-channel in stenosed arteries and also in high-throughput microfluidics systems, we intend to present numerical results at moderate Reynolds numbers typical of the aforementioned applications.

The paper is organized as follows: We start by presenting the governing equations for steady, laminar, incompressible, and isothermal flow of Phan-Thien/Tanner fluids between two parallel plates partially obstructed by a symmetric cosinusoidal constriction. We then proceed with briefly describing the finite volume method (OpenFoam) used for numerical solution of these equations. Typical numerical results are presented next depicting the role played by different model parameters on the flow characteristics. The paper is concluded by highlighting its major findings.

2. Mathematical Formulation

We consider laminar flow of an incompressible viscoelastic fluid obeying the Phan-Thien/Tanner model in a

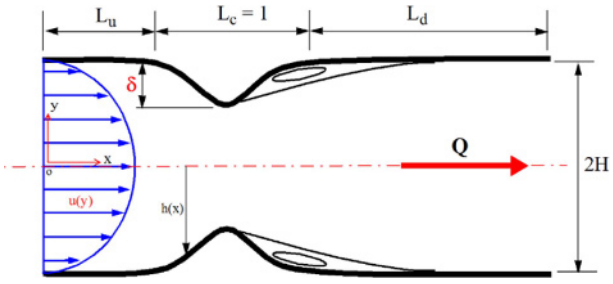

Fig. 1. (Color online) Schematic showing a typical planar, cosinusoidal constricted channel (diagram not to scale).

planar partially-constricted symmetric channel of height 2H, as shown schematically in Fig. 1. This figure also shows the Cartesian coordinate system used for the mathematical development. The height of the minimum area of the constriction (say, the throat) is equal to $2H_0$. The constriction has a length equal to L_c which is arbitrarily set equal to "one". Like Cheng (1972) and Mahapatra *et al.* (2002) the constriction is assumed to be the following cosinusoidal shape:

$$h(x) = H - \frac{\delta}{2}\{1 - \cos[2\pi(x - L_u)]\} \tag{1}$$

where δ is the height of the minimum area of the channel. It is worth-mentioning that in current converging-channel extensional rheometers, the profile of the constriction is not trigonometric. In fact, it is shaped in such a way that the rate of extension is virtually constant along the channel (Wang and James, 2011). The simple geometry chosen for the analysis in the present work (see Eq. (1)) is quite easy to fabricate/implement in current microfluidic systems in future experimental studies. There is also no doubt that it better represents stenosed arteriesy in human body as compared with the orifice plate used by Tamaddon-Jahromi *et al.* (2011). This geometry is also good for code-verification purpose noting, the fact that published data are available for Newtonian fluids in this particular geometry (Cheng, 1972; Mahapatra *et al.*, 2002). To that end, like Cheng (1972) and Mahapatra *et al.* (2002), the flow is assumed to be steady, laminar, incompressible, isothermal, two-directional, and two-dimensional; gravity effects are also neglected.

2.1. Equations of motion

Excluding any gravitational and thermal effects, in vectorial form, the momentum equations together with the continuity equation can be written as,

$$\rho\frac{D\mathbf{u}}{Dt} = -\nabla p + \nabla\cdot\boldsymbol{\tau}, \tag{2a}$$

$$\nabla\cdot\mathbf{u} = 0 \tag{2b}$$

where D/Dt is the material derivative, ρ is the fluid's density, p is the isotropic pressure, $\mathbf{u}$ is the velocity vector, and $\boldsymbol{\tau}$ is the stress tensor. For polymeric liquids, the stress tensor can be divided into solvent contribution and polymer contribution; that $\boldsymbol{\tau} = \boldsymbol{\tau}_s + \boldsymbol{\tau}_p$ where the first part is the viscous stress contributed by the solvent (say, water) and the second parts is that contributed by the constituent (say, polymer chains). For Newtonian solvent, we have: $\boldsymbol{\tau}_s = \eta_s\mathbf{D}$ where η_s is the solvent viscosity, and $\mathbf{D} = \nabla\mathbf{u} + \nabla\mathbf{u}^T$ is the rate-of-deformation tensor with $\nabla\mathbf{u} = \partial u_j/\partial x_i$ being the velocity gradient tensor. As to the elastic stress contributed by the polymer chains, we assume that it can be calculated using the Phan-Thien/Tanner (PTT) model. This fluid model has been derived originally for polymeric melts based on the idea that polymer chains can interact with each other in such a way that they can form transient networks giving rise to the fluid's viscoelasticity. The constitutive equation for this fluid model reads as (Phan-Thien and Tanner, 1977; Phan-Thien, 1978),

$$g(\boldsymbol{\tau})\boldsymbol{\tau} + \lambda\overset{\square}{\boldsymbol{\tau}} = \eta_p\mathbf{D} \tag{3}$$

where λ is the relaxation time, and η_p is the viscosity contributed by the solute (say, polymer chains) to the total zero-shear viscosity of the solution: $\eta_0 = \eta_s + \eta_p$, with η_s being the viscosity contributed by the solvent. In Eq. (3), $\overset{\square}{\boldsymbol{\tau}}$ is the Gordon-Schowalter convected derivative which is defined as (Bird *et al.*, 1987; Larson, 1988):

$$\overset{\square}{\boldsymbol{\tau}} = \frac{D}{Dt}(\boldsymbol{\tau}) - (\boldsymbol{\tau}\cdot\nabla\mathbf{u} + \nabla\mathbf{u}^T\cdot\boldsymbol{\tau}) + \xi(\boldsymbol{\tau}\cdot\mathbf{D} + \mathbf{D}\cdot\boldsymbol{\tau}) \tag{4}$$

where D/Dt is the material derivative, ξ is the slip parameter (representing the non-affine deformation of polymer chains in the continuum) which is related to the effective velocity gradient tensor as: $\mathbf{L} = \nabla\mathbf{u} - \xi\mathbf{D}$ with u being the velocity vector and $\mathbf{D}$ the rate-of-deformation tensor. As noted by Saramito (1995) the Gordon-Schowalter derivative suffers from the problem that it can give rise to a maximum in the flow-curve of the fluid. This maximum has never been observed experimentally for any polymeric liquid and results in a discontinuity in the velocity profile in Poiseuille flow. As such, we have decided to set $\xi = 0$ in this work. By so-doing the Gordon-Schowalter convected derivative is reduced to the upper-convected derivative. Also, the reduced model (which is called the simplified Phan-Thien/Tanner model or SPTT) cannot predict a non-zero second normal stress difference (N2). The failure of the model in predicting N2 cannot be regarded as a drawback in this work because, as earlier mentioned, N2 plays no role on the pressure drop in constricted-channel flows.

As to the stress coefficient function, $g(\boldsymbol{\tau})$, in Eq. (3) it must be said that it has a linear form and an exponential form (Phan-Thien and Tanner, 1977). The linear form allows the extensional viscosity to be bounded whereas

the exponential form is good for fluids exhibiting a maximum in their extensional viscosity followed by strain-softening at larger extension rates. Both forms have been realized to fit the data for certain polymeric materials and concentrated polymer solutions (Phan-Thien and Tanner, 1977). In the present work, we are primarily interested in the linear version of the model as it is the same model used by Tamaddon-Jahromi *et al.* (2011); it reads as:

$$g(\boldsymbol{\tau}) = 1 + \frac{\varepsilon\lambda}{\eta_p}\,\mathrm{trace}(\boldsymbol{\tau}). \tag{5}$$

It is worth-mentioning that, the linear SPTT model is often referred to as LPTT. In this model, ε is called the extensional parameter - simply because it has a strong effect on the extensional-flow behavior of the material. Although, in principle, this parameter lies in the range of [0,1], for the model to represent strain-hardening fluids, this dimensionless parameter should be smaller than roughly 0.5 (Grillet *et al.*, 2002). In fact, for most polymeric melts and concentrated polymer solutions it is realized to be less than 0.25; see Phan-thien and Tanner (1977), Xue *et al.* (1998), and Oliveira and Pinho (1999). The rheological behavior of the LPTT model is obviously controlled by three material properties: (λ, ε, η_p). For a given zero-shear viscosity (say, one) an increase in the solute contribution means a decrease in the solvent contribution, and vice versa. With the zero-shear-viscosity being fixed, the retardation parameter, $\beta = \eta_p/\eta_0$ (also called the solute viscosity ratio) can be used as an independent parameter to represent the solution (Xue *et al.*, 1998). Based on this definition, $\beta = 0$ means pure solvent and $\beta = 1$ means a polymer melt. So, all in all, our fluid mechanics problem involves three material parameters: λ, ε, and β. While the last two are dimensionless by default, the first one can be expressed as a dimensionless number (say, the Deborah number). In the present work, the separate effects of these three material properties are investigated on the excess pressure drop for a LPTT fluid.

To close the problem, we need appropriate boundary conditions at the inlet, outlet, the symmetry plane, and also at the walls of the channel. As to boundary conditions, at the inlet we can prescribe the analytical solution obtained recently by Alves *et al.* (2001) for plane Poiseuille flow of LPTT fluids - that solution was for $\beta = 1$ but it could easily be extended to any other β albeit semi-analytically (not shown here). The stress tensor corresponding to these fully-developed velocity profiles can be used as the stress boundary conditions at the inlet. At the outlet, the transverse velocity is set equal to zero together with the gradient of the axial velocity and all stress terms. Along the symmetry plane, the gradient of the axial velocity (u) in the y-direction is set equal to zero while the cross-stream velocity component (v) is forced to be equal to zero. At all solid walls, no-slip and no-penetration conditions are imposed on both velocity components (u, v). Also, the gradients of all stress terms are set equal to zero at the walls. As to the pressure, it is set equal to zero at the inlet section of the channel in all simulations. The pressure at the outlet is what we compute in the course of the computations.

A solution of the equations of motion subject to these boundary conditions can provide us with the pressure variation along the channel from which we can determine the "excess pressure drop" (*epd*), if needed. For Boger fluids, Nyström *et al.* (2016) and Tammadon-Jahromi *et al.* (2016) defined it as:

$$epd = \frac{(\Delta p - \Delta p_{\mathrm{fd}})_B}{(\Delta p - \Delta p_{\mathrm{fd}})_N} = \frac{\Delta p_B}{\Delta p_N} \tag{6a}$$

where the subscripts "B" and "N" represent the contribution by the Boger fluid and its Newtonian baseline, respectively. In this relationship Δp is the total pressure drop (*i.e.*, the pressure difference between the inlet and outlet sections of the channel (say, far upstream and far downstream of the constriction; see Fig. 1), and $\Delta p_{fd} = \Delta p_u L_u + \Delta p_d L_d$ is the pressure drop associated with the fully-developed sections of the channel at each side of the constriction. As previously mentioned, based on experimental observations, this ratio is larger than one for Boger fluids.

The above definition for *epd* is definitely a legitimate one for Boger fluids. But, it fails to predict an *epd* for certain other types of viscoelastic fluids. In our opinion, for shear-thinning viscoelastic fluids the definition of *epd* needs to be revised. This is because for such fluids the pressure drop associated with the constriction consists of the pressure drop due to shearing (Δp_{sh}) and that due to stretching (Δp_{ext}). Unlike Δp_{ext} which can be determined either experimentally or numerically (Wang and James, 2011), the pressure drop associated with shearing, Δp_{sh}, can only be determined through a numerical analysis (James *et al.*, 1990). This is because to determine Δp_{sh}, we need a fluid which is *inelastic* but shows a shear-thinning behavior similar to that of the original viscoelastic fluid. No such a fluid does exist in the real world simply because the same mechanism which gives rise to shear-thinning also gives rise to the fluid's elastic behavior. To circumvent this problem, the best we can do is to fit a power-law curve to the viscosity data of the viscoelastic fluid at hand (say, LPTT fluid), and then redo the simulation for this inelastic analogue. A proper definition for excess-pressure-drop valid for shear-thinning viscoelastic fluids appears to be the following relationship:

$$epd = \frac{(\Delta p - \Delta p_{fd})_{PTT}}{(\Delta p - \Delta p_{fd})_{in}} = \frac{\Delta p_{ext} + \Delta p_{sh}}{\Delta p_{sh}} > 1 \tag{6b}$$

where Δp_{ext} is the pressure drop due to stretching and Δp_{sh} is that due to shearing. In the above definition, the

subscript "in" refers to the inelastic analogue of the original viscoelastic fluid. This definition guarantees that, as long as the fluid is strain-hardening/shear-thinning *epd* always stays above one. With this in mind, the numerical results reported by Tammadon-Jahromi *et al.* (2011) showing that LPTT fluids the excess-pressure-drop is lower than its Newtonian counterpart can be attributed to an unwarranted use of Eq. (6a) which is based on Newtonian baseline. That is to say that, while use should have been made of Eq. (6b) for this purpose which is based on power-law baseline. At this stage, we would like to stress that in the present work, we do not intend to get involved with measuring/predicting the extensional viscosity of any viscoelastic fluid using *epd* data. We only wanted to show that the LPTT model can correctly predict *epd* provided that an appropriate baseline is implemented in its definition. For completeness, however, in Appendix A we have briefly explained how excess-pressure-drop and pressure-drop data can be used to extract a fluid's extensional viscosity.

In the next section we briefly describe the numerical method employed to compute the pressure drop for the LPTT fluid. But, to reduce the number of parameters involved in the problem, first the governing equations are made dimensionless through invoking appropriate measures for length, velocity, pressure, and stress terms. To that end, we substitute:

$$(x^*, y^*, \delta^*) = \frac{(x, y, \delta)}{H}; (u^*, v^*) = \frac{(u, v)}{U}; p^* = \frac{p}{\rho U^2};$$
$$\tau_{ij}^* = \frac{\tau_{ij}}{(\eta_0 U/H)} \quad (7)$$

where U is the average velocity. It is worth mentioning that, the way by which stress terms have been made dimensionless is different from that used for the pressure terms. This cannot be regarded as a drawback of our dimensional analysis simply because no true scaling is actually involved in the present work. That is to say that, no approximate theory such as creeping-flow theory or boundary-layer theory is invoked in this work in order to ignore any term(s) in the equations of motion in comparison with other terms. All in all, the problem is governed by the following dimensionless parameters: The Reynolds number (Re), the Deborah number (De), the retardation parameter (β), and the blockage ratio (δ). They are defined as follows:

$$Re = \frac{\rho UH}{\eta_0}, \quad (8a)$$

$$De = \frac{\lambda}{(H/U)}, \quad (8b)$$

$$\delta^* = \frac{\delta}{H} \quad (8c)$$

where the Deborah number (De) can be deemed as the dimensionless relaxation time. Another dimensionless number involved is the extensional parameter, ε, as earlier mentioned. In the next section, the numerical method adopted for carrying out the simulation is briefly described. For convenience, the asterisks above all dimensionless parameters would be dropped henceforth.

3. Numerical Method

In the present study, an open-source software called OpenFoam has been used to solve the governing equations for our LPTT fluid. In a stimulating work, Favero *et al.* (2010) have developed a robust module called ViscoelasticFluidFoam solver which has enabled OpenFOAM software to handle a variety of viscoelastic fluid models such as LPTT (see also Pimenta and Alves (2017) and Fernandes *et al.* (2019)). The solver has been shown to accurately reproduce the numerical data for this fluid model in several benchmark problems including the 4:1 contraction flow (Favero *et al.*, 2010). OpenFOAM is a finite-volume software in which the second-order central difference (CDS) scheme is used to discretize the diffusion and divergence terms. The same scheme is also used for discretizing the pressure-gradient terms in the momentum equations. In this robust scheme the flux value for any quantity on the surface of a control volume is calculated from a linear interpolation of its value on the center of the cells located on each side of that particular surface.

A major challenge when dealing with viscoelastic fluid flows is the discretization of the advection terms, and this is particularly so at high Deborah numbers. To avoid numerical instability at high Deborah numbers, in the literature, use is often made of the the upwind method for discretizing the advection terms. In practice, this simple method discretizes the advection terms in a direction corresponding to the characteristic velocity for information propagation. (That is to say that, the advection terms are discretized by using a difference which is biased towards the direction determined by the sign of its coefficient multiplied by the advection term.) The disadvantage of this simple upwind scheme is that it is a first-order order scheme and this might give rise to false diffusion. To circumvent this problem, the ViscoelasticFluidFoam solver of the OpenFoam relies on the MINMOD method (Harten, 1983) for discretizing the advection terms for viscoelastic fluid models. This scheme combines the advantages of the CDS with that of the upwind scheme and works fine at moderate Deborah numbers. MINMOD is a flux limiter method in which the discritization direction is determined by the magnitude of the flux. This means that we dicretize the advection terms in such a way that the flux becomes smaller in that direction.

As the first task, we had to ensure that the numerical

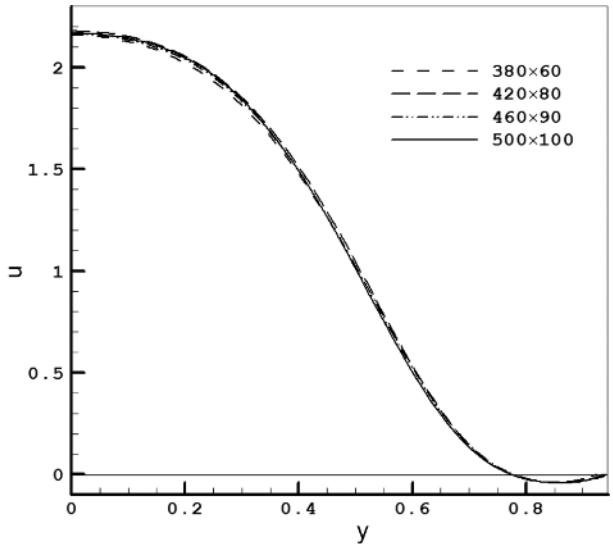

Fig. 2. Effect of the grid size on the velocity profile of LPTT fluid flowing through the channel shown in Fig. 1 (x = 15, Re = 50, De = 1, ε = 0.25, β = 0.7, and δ = 0.5).

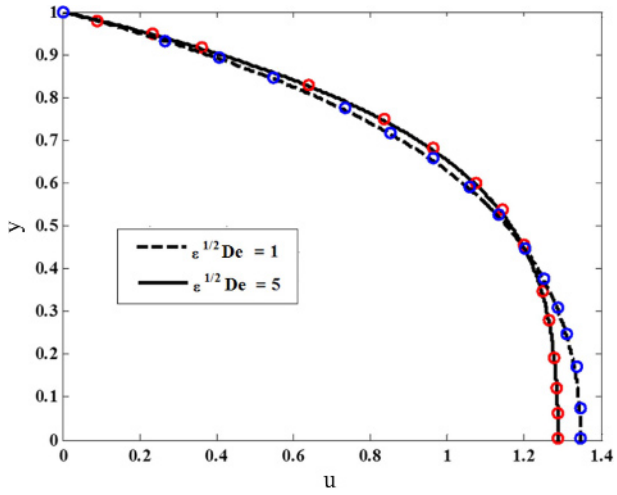

Fig. 3. (Color online) A comparison between numerical results obtained using OpenFoam (shown by lines) with the analytical solution reported by Oliveira and Pinho (1999) (shown by symbols) for the velocity profiles in plane Poiseuille flow of LSPTT fluids (Re = 1, β = 1).

results are grid-independent. To that end, four different grids of 380×60, 420×80, 460×90, and 500×100 have been tried. Figure 2 shows the effect of the grid size on the dimensionless velocity profile computed obtained at the largest Reynolds number tried in this work (*i.e.*, Re = 50) at the throat. As can be seen in this figure, grid-independent results can be achieved for this demanding test case (which exhibits flow reversal) using the 460×90 mesh. To be on the safe side, we have decided to rely on a 500×100 mesh for the rest of the work. As earlier mentioned, our main concern is to determine the pressure variation along the channel in order to see if there exists any "excess pressure drop" as compared with its Newtonian counterpart.

3.1. Code verification

To verify the numerical scheme, OpenFoam is used to reproduce the analytical velocity profiles long established in the literature for LPTT fluids in plane Poiseuille flow at β = 1. As can be seen in Fig. 3, the numerical results are in good agreement with the analytical data reported in the literature; see Oliveira and Pinho (1999). We have easily extended their results to other β values using a semi-analytical approach (not shown here). Figure 4 shows such velocity profiles.

To further verify the numerical scheme, we have tried to reproduce the axial velocity profiles reported by Azaeiz *et al.* (1996) for LPTT fluids in a 4:1 plane contraction flow, shown schematically in Fig. 5. Their finite-element (FEM) results have been compared with our FVM results obtained using OpenFoam in Fig. 6. As can be seen in this figure, the two sets of results are virtually the same confirming that OpenFoam is well capable of dealing with

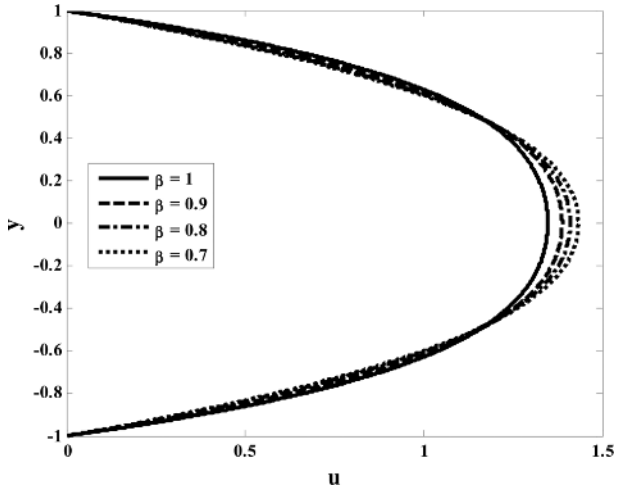

Fig. 4. Effect of the retardation parameter, β, on the velocity profiles of LPTT fluids in plane Poiseuille flow (ε = 0.25, De = 2).

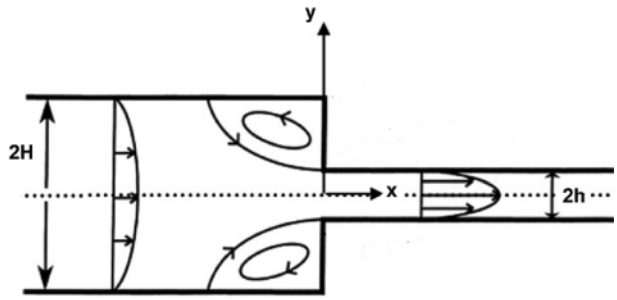

Fig. 5. Schematic showing the 4:1 planar contraction flow used by Azaiez *et al.* (1996).

LPTT fluid flows in contracted channels.

As a more demanding test, we have tried to reproduce

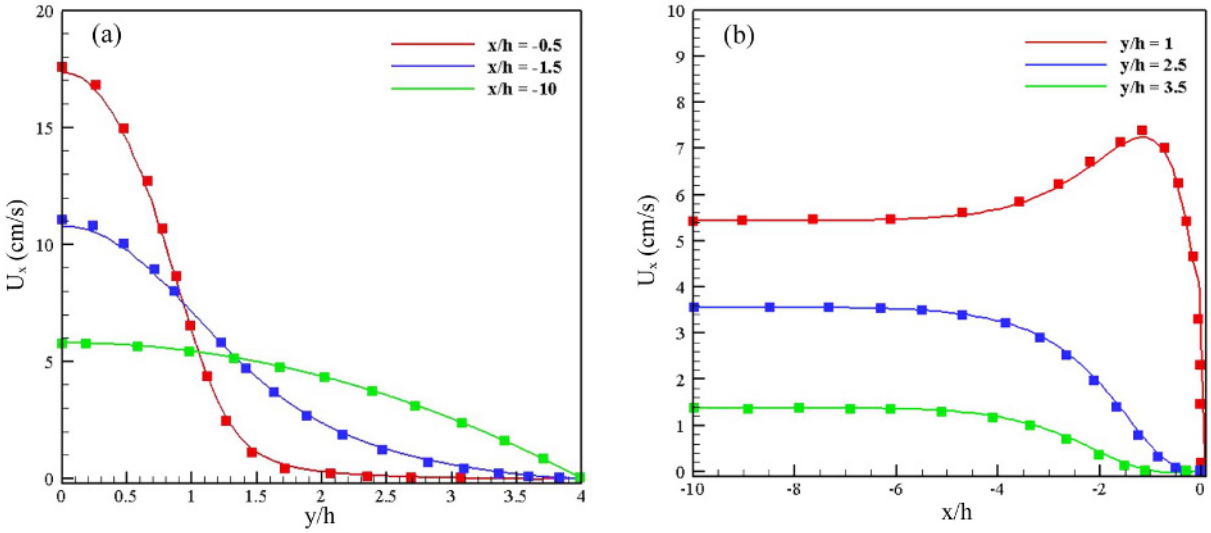

Fig. 6. (Color online) A comparison between our OpenFoam (shown by lines) with the FEM results (shown by symbols) obtained by Azaiez *et al.* (1996) for LPTT fluid flowing through a 4:1 contraction: (a) The axial velocity profiles at different cross-sections, (b) variation of the axial velocity along the channel at different distances from the centerline (Re = 0.56, De = 1.45, β = 1, and ε = 0.25).

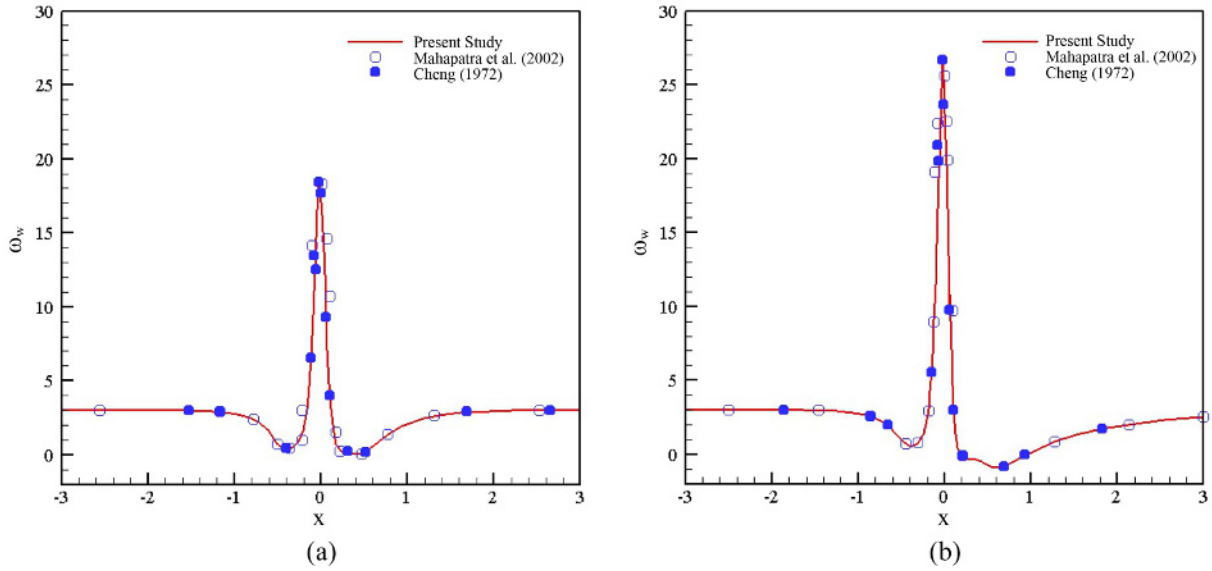

Fig. 7. (Color online) A comparison between the numerical results obtained using OpenFoam for Newtonian fluids (shown by line) with the numerical results reported in Mahapatra *et al.* (2002) (show by symbol) for the variation of wall vorticity for a 40% blockage ratio obtained for $L_u = L_d$ = 2.5, and L_c = 1: (a) Re = 10, and (b) Re = 25.

Newtonian results obtained by Cheng (1972), and Mahapatra *et al.* (2002) in a constricted channel of cosinusoidal shape. As can be seen Fig. 7, the performance of OpenFoam is very good in reproducing Newtonian results in this challenging fluid mechanics problem.

In the next section, we present the numerical results obtained using OpenFoam for LPTT fluids in the constricted channel depicted schematically in Fig. 1. We are primarily interested in investigating the effect of the material properties on the pressure drop. To that end, we are going to fix the Reynolds number and also the blockage ratio and obtain numerical results for different values of De, ε, and β. To proceed with the numerical simulation, we have to decide on the geometrical parameters of the channel. To that end, we typically set: L_u = 13.5H, L_c = H, and L_d = 25.5H so that the total length of the channel is equal to 40H. With no loss of generality, like Cheng (1972), we arbitrarily set H = 1 in our analysis even though. Thus the minimum area is located at x_0 = 14. Thanks to the symmetry assumption, it suffices to consider only half of the channel (say, the upper half) as the computational domain. As the first task, we have to draw

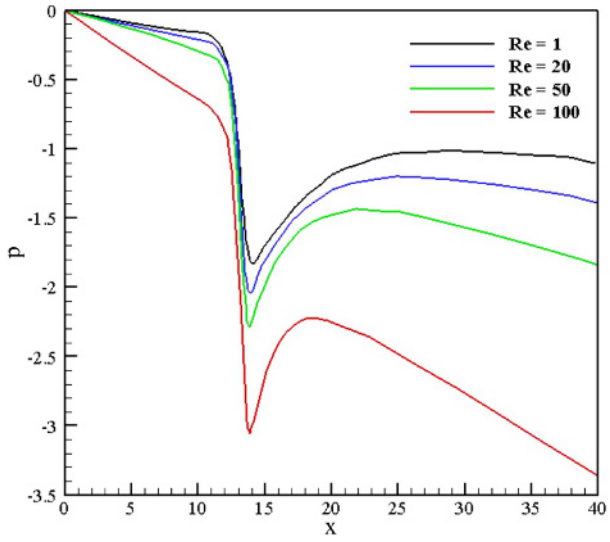

Fig. 8. (Color online) Dimensionless pressure variation along the centerline of the channel at different Reynolds numbers obtained for a Newtonian fluids in the channel shown schematically in Fig. 1 ($\beta = 0.2$, $\delta = 0.5$).

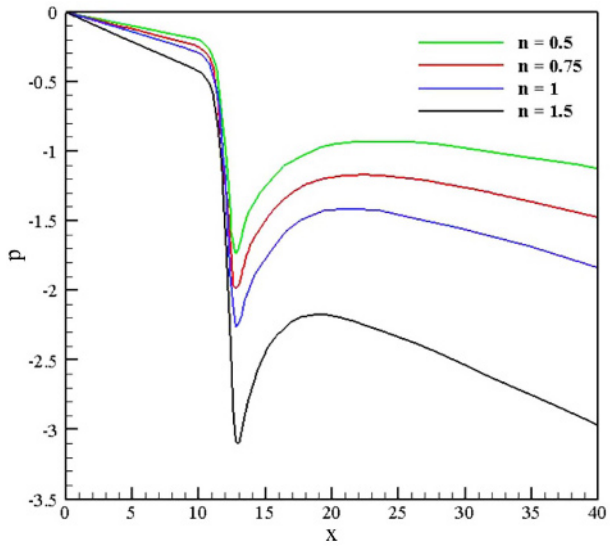

Fig. 9. (Color online) Effect of the power-law index on the pressure variation along the centerline of the channel shown schematically in Fig. 1 ($Re = 50$, $\delta = 0.5$).

a baseline with which to assess the size of the elastic effects. For Boger fluids, use can be made of Newtonian baseline for calculating the *epd* (Tammadon-Jahromi *et al.*, 2011). Figure 8 shows typical pressure-drop profiles obtained at different Reynolds numbers to be used as Newtonian baseline. For LPTT fluids, because of their shear-thinning behavior, a purely-viscous power-law baseline appears to be a better idea. Figure 9 shows a typical pressure drop baseline obtained using power-law curve-fitting to the viscosity profile of LPTT fluids.

4. Results and Discussion

In this section, we present our numerical results obtained for LPTT fluids in their flow through the constricted channel depicted schematically in Fig. 1. As earlier mentioned, our main interest lies in investigating the effect of the material properties (λ, β, and ε) on the pressure drop experienced by the fluid. In dimensionless form, this means that we have to study the effect of Deborah number (De), the extensional parameter (ε), and the retardation parameter (β). For curiosity, the effect of the con-

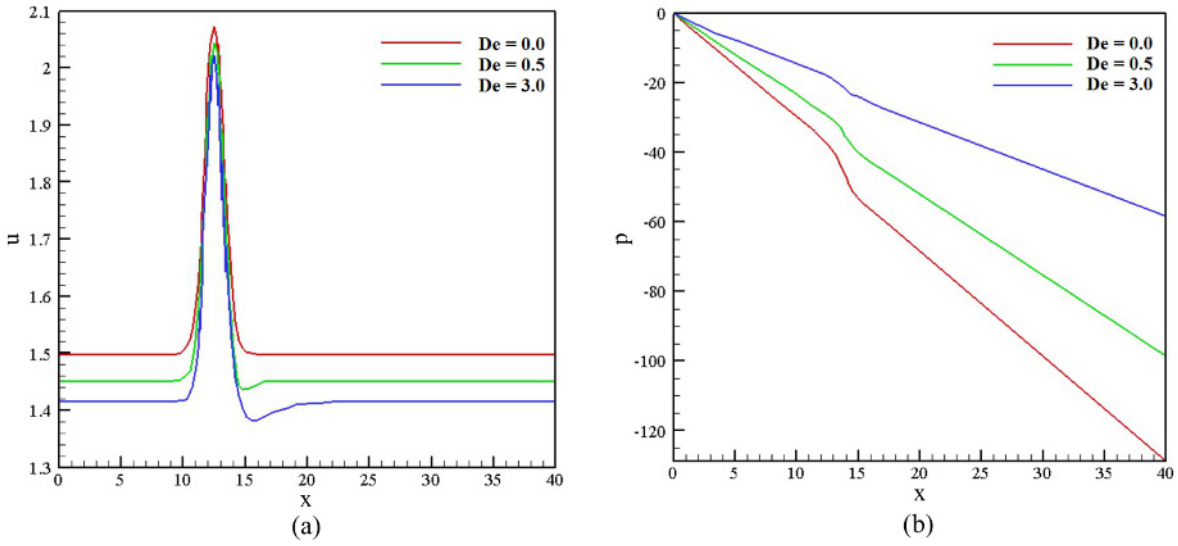

Fig. 10. (Color online) Effect of the Deborah number on the dimensionless centerline axial velocity and pressure variations for LPTT fluids. The pressure is minimum at the throat ($x_0 = 14$) and is decreased when Deborah number is increased ($Re = 1$, $\varepsilon = 0.25$, $\beta = 0.7$, and $\delta = 0.3$).

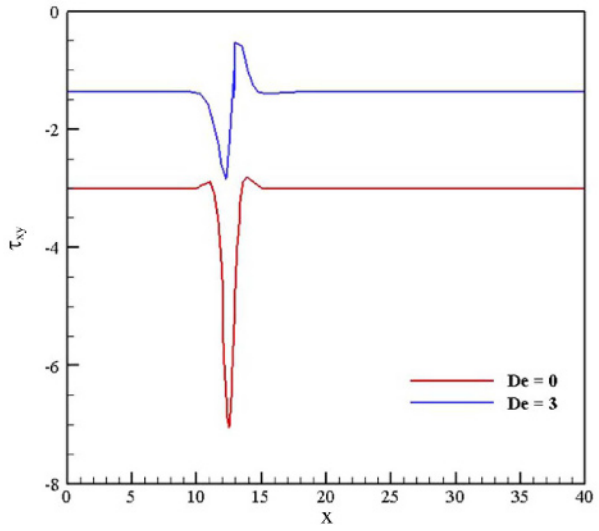

Fig. 11. (Color online) Effect of the Deborah number on the shear stress experienced by the fluid at the wall (Re = 1, ε = 0.25, β = 0.7, and δ = 0.3).

striction's dimensionless geometrical parameters (δ and L_c) is also investigated in Appendix C. It needs to be stressed from this point onward all parameters to be used in the numerical results are dimensionless.

4.1. Effect of the Deborah number

Figure 10 shows the effect of the Deborah number on the dimensionless velocity and pressure variation along the centerline of the channel obtained at Re = 1. This figure shows that the axial velocity and pressure are both decreased when the Deborah number is increased. These predictions are consistent with the notion that by an increase in the Deborah number, the fluid becomes slightly more shear-thinning which starts at lower shear rates (see Appendix B). This makes the velocity profile flatter with its value dropped at the centerline. On the other hand, the drop in viscosity is sufficient to lower the wall shear stress, as can be seen in Fig. 11. A drop in the wall shear stress means that the fluids need a lower pressure drop to pass through the constriction. But, shear stress is not the only influential parameter involved in this problem. Another parameter which has a decisive role is the first normal-stress-difference in extension $(\tau_{xx} - \tau_{yy})_{ext}$ which is directly proportional to the fluid's extensional viscosity. Figure 12 shows the variation of the two normal stress components (τ_{xx} and τ_{yy}) along the centerline of the channel where there is no shear stress. This figure shows that while τ_{xx} is an increasing function of the Deborah number, τ_{yy} is decreasing with De number. More importantly, $(\tau_{xx} - \tau_{yy})_{ext}$ is predicted to increase when the Deborah number is increased. The effect of extensional viscosity is known to increase the pressure drop. The two effects (*i.e.*, shear-thinning and strain-hardening) obviously work in the opposite directions. The prediction that the net pressure drop is decreased by an increase in the Deborah number (see Fig. 10) suggests that the effect of shear-thinning is stronger than the effect of the fluids strain-hardening, at least for this set of parameters.

From the pressure-drop data presented in Fig. 10, we can easily extract the "*epd*" data for LPTT fluids. Figure 13a shows that the *epd* data obtained using Eq. (6a). It shows that by an increase in the Deborah number, *epd* drops, as previously noted by Tammadon-Jahromi *et al.* (2011). In their paper, they have argued that the overstrong effect of shear-thinning is dominating the effect of the first-normal-stress difference giving rise to a drop in *epd*. No shear stress and/or first-normal-stress difference data have been provided by them in the constriction region to support their argument. It is not even clear if by first

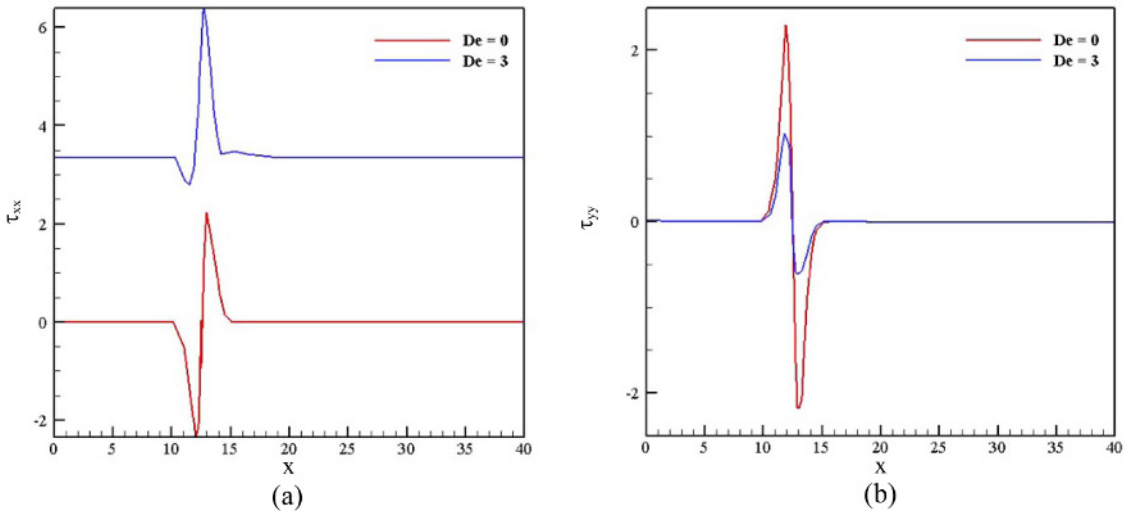

Fig. 12. (Color online) Effect of Deborah number on the normal stresses developed in the fluid along the channel's centerline (Re = 1, ε = 0.25, β = 0.7, and δ = 0.3).

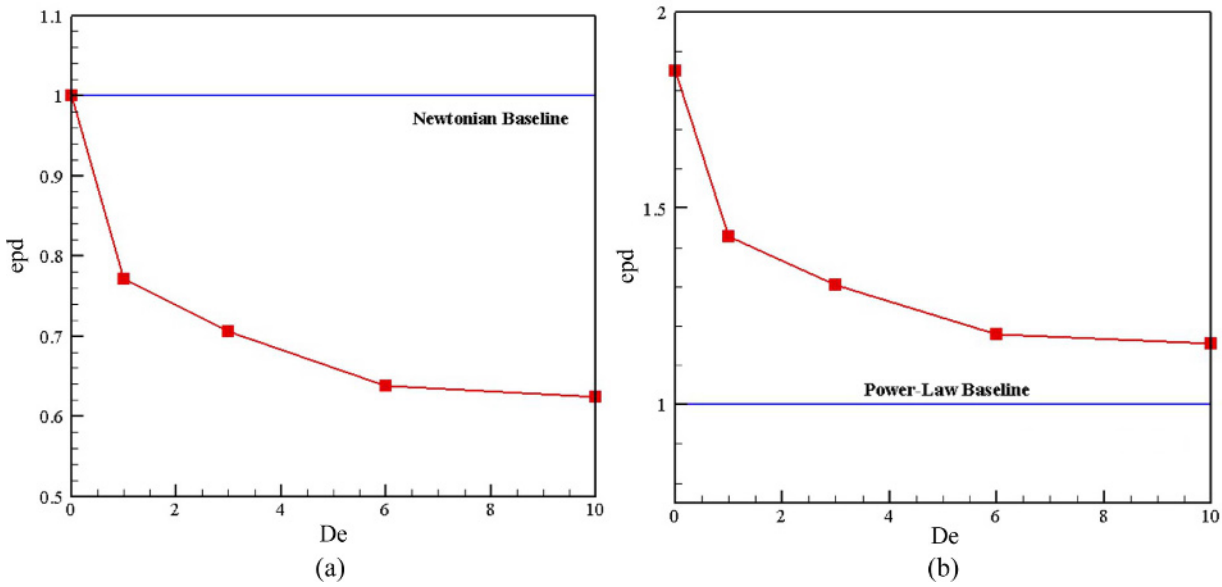

Fig. 13. (Color online) Variation of the normalized excess-pressure-drop with Deborah number ($\varepsilon = 0.25$, $\beta = 0.7$, and $\delta = 0.3$), (a) based on Eq. (6a) and (b) based on Eq. (6b).

normal-stress-difference they have meant $(\tau_{xx} - \tau_{yy})_{ext}$ or N1. We have already argued that for shear-thinning viscoelastic fluids such as LPTT, the correct baseline is the one based on an inelastic analogue of the original fluid (say, obtained, using the power-law fit to the viscosity data of LPTT fluids); see Eq. (6b). As can be seen in Fig. 13b, such a power-law baseline guarantees that an excess pressure drop can indeed be predicted for LPTT fluid albeit it is still a decreasing function of the Deborah number again, demonstrating the strong role played by the shear-thinning aspect of the LPTT fluids on the pressure drop, as noted by Tammadon-Jahromi *et al.* (2011).

All in all, the effect of the Deborah number is as follows: i) The axial velocity is decreased, ii) the pressure drop is decreased, iii) the wall shear stress is decreased, and iv) the first normal stress difference (in extension) is increased.

4.2. Effect of the extensional parameter

Figure 14 shows the effect of extensional parameter on the centerline velocity and centerline pressure variation. The effect of ε is seen to be qualitatively similar to the effect of the Deborah number. That is to say that both are decreased when this parameter is increased. This is not

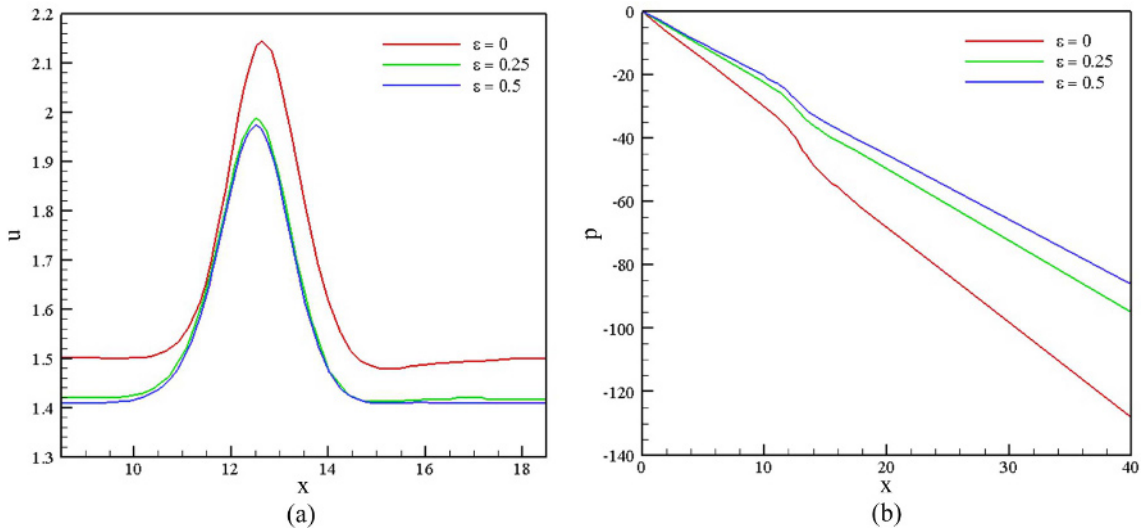

Fig. 14. (Color online) Effect of the extensional parameter on the dimensionless velocity profile and centerline pressure variation ($De = 0.5$, $Re = 1$, $\varepsilon = 0.25$, $\beta = 0.7$, and $\delta = 0.3$).

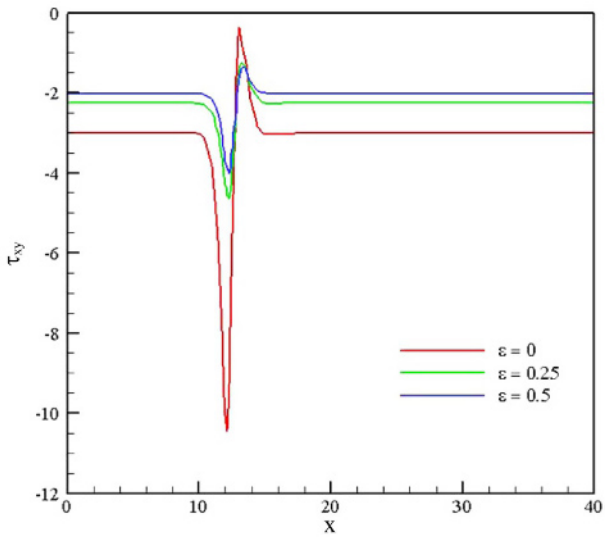

Fig. 15. (Color online) Effect of the extensional parameter on the dimensionless wall shear stress (De = 0.5, Re = 1, ε = 0.25, β = 0.7, and δ = 0.3).

surprising in realizing the fact that by an increase in ε shear-thinning starts at lower shear rate. So, for a given shear rate, viscosity and therefore the wall shear stress is lower (see Fig. 15). Thus, the velocity becomes flatter so that its value at the centerline is lowered. This by itself lowers the pressure drop. A further recovery in pressure is caused by $(\tau_{xx} - \tau_{yy})_{ext}$ which is dropped by an increase in the extensional parameter (see Fig. 16). Both effects work in the same direction, and so the pressure is recovered by an increase in this parameter. Still, the pressure recovery is not as much when compared with the effect of Deborah number. This is because the effect of ε on shear-thinning is weaker than the effect of Deborah number.

All in all, the effect of the extensional parameter is as follows: i) The axial velocity is decreased, ii) the pressure drop is decreased, iii) the wall shear stress is decreased, and iv) the first normal stress difference (in extension) is increased.

4.3. Effect of the retardation parameter

Figure 17 shows the strong effect of the retardation parameter on the centerline velocity profile and pressure variation along the channel. The effect of β is seen to be quite similar to the effect of the Deborah number and also the extensional parameter. That is to say that, as far as pressure drop is concerned, by an increase in β the pressure drop is decreased. This is not surprising in realizing the fact that for a given η_s by an increase in β the fluid becomes progressively more shear-thinning. Therefore, the wall shear stress should decrease, as can be seen in Fig. 18. As mentioned above, this has an accelerating effect on the fluid elements near the wall so that the pressure drop is decreased. But, as can be seen in Fig. 19, $(\tau_{xx} - \tau_{yy})_{ext}$ is increased when β is increased which increases the pressure drop. The net effect is predicted to be that of acceleration so much so that the pressure drop is overall decreased (see Fig. 18).

All in all, the effect of the retardation parameter is as follows: i) The axial velocity is decreased, ii) the pressure drop is decreased, iii) the wall shear stress is decreased, and iv) the first normal stress difference (in extension) is increased.

4.4. High Reynolds-number results

The above results have been obtained at a typically low Reynolds number of "one". Working at low Reynolds number has the advantage that no end effects are involved. It also means that viscous stresses are as important as the

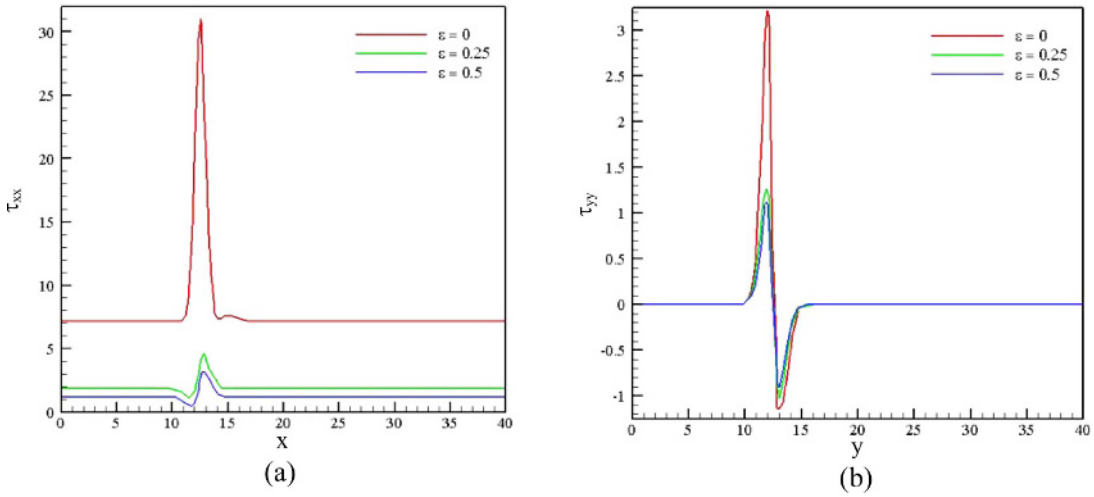

Fig. 16. (Color online) Effect of the extensional parameter on the dimensionless centerline normal stress (De = 0.5, Re = 1, ε = 0.25, β = 0.7, and δ = 0.3).

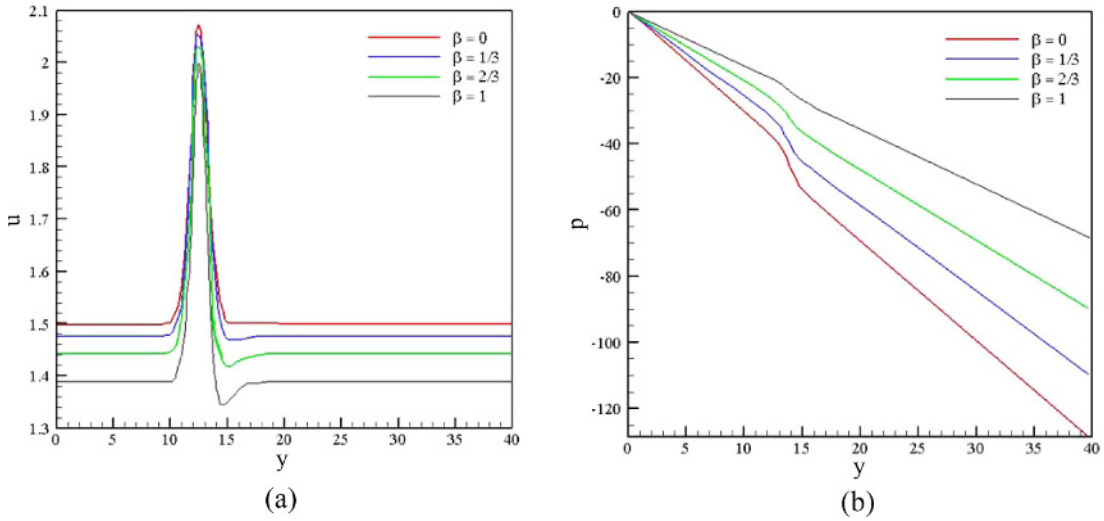

Fig. 17. (Color online) Effect of the retardation parameter, β, on the dimensionless centerline velocity and centerline pressure variation (Re = 1, De = 0.5, ε = 0.25, and δ = 0.3).

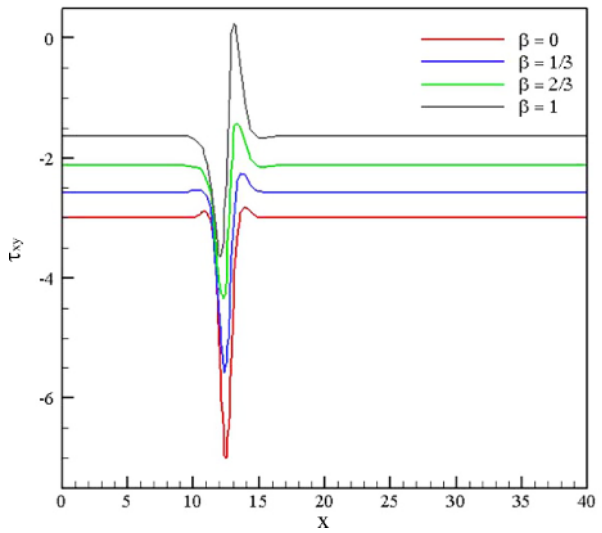

Fig. 18. (Color online) Effect of the retardation parameter, β, on the dimensionless wall shear stress distribution (Re = 1, De = 0.5, ε = 0.25, and δ = 0.3).

elastic stresses is giving rise to excess pressure drop. This is perhaps why virtually all extensional rheometers in current use work at low Reynolds numbers (see, for example, Wang and James (2011)) while in the past the perception was to operate such devices at high Reynolds numbers - not a good idea because the instrument was dependent on the pressure-drop data obtained numerically for an equivalent power-law analogue of the viscoelastic fluid at hand. As previously mentioned, in the present work we are not actually concerned with the measurement of the extensional viscosity for any fluid. Still, we have tried to obtain results at medium Reynolds numbers due mainly to their application in physiological systems (for example, when blood has to flow through stenosed arteries; see, Giddens

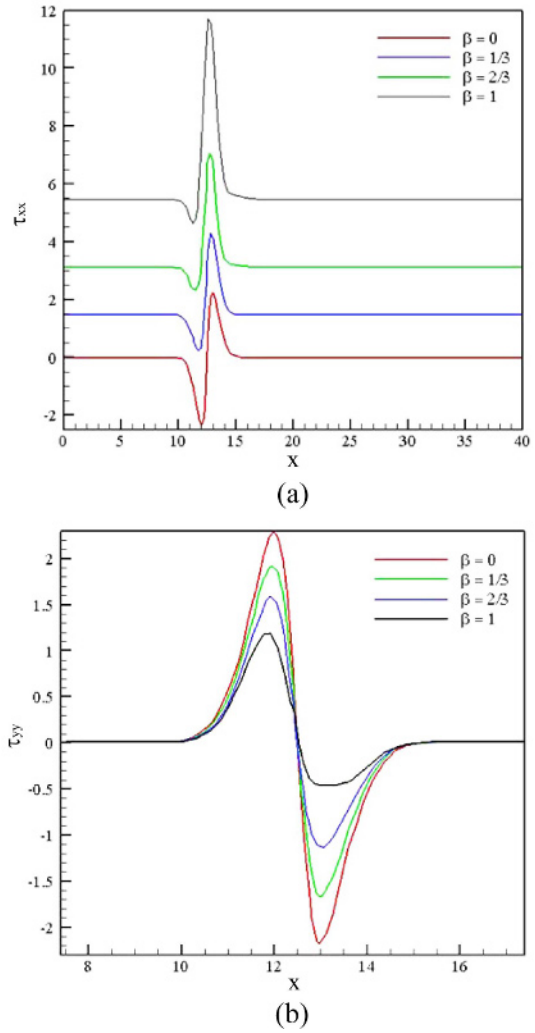

Fig. 19. (Color online) Effect of the retardation parameter, β, on the dimensionless centerline normal stress components (Re = 1, De = 0.5, ε = 0.25, and δ = 0.3).

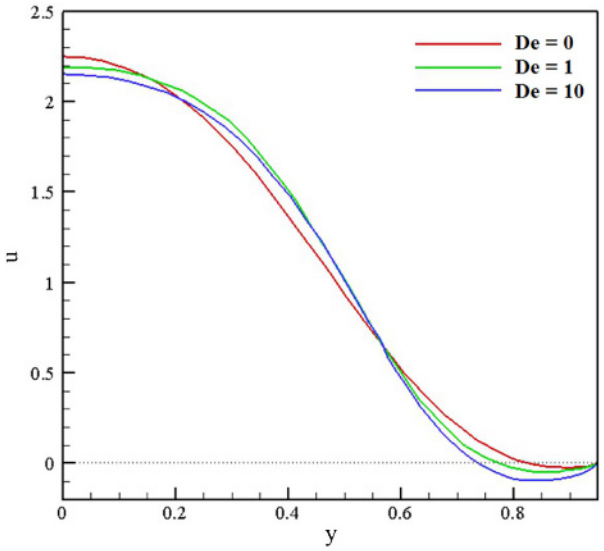

Fig. 20. (Color online) Effect of Deborah number on the velocity profile downstream of the throat. The flow reversal is evident in this figure (x = 14, Re = 50, ε = 0.4, β = 0.7, and δ = 0.5).

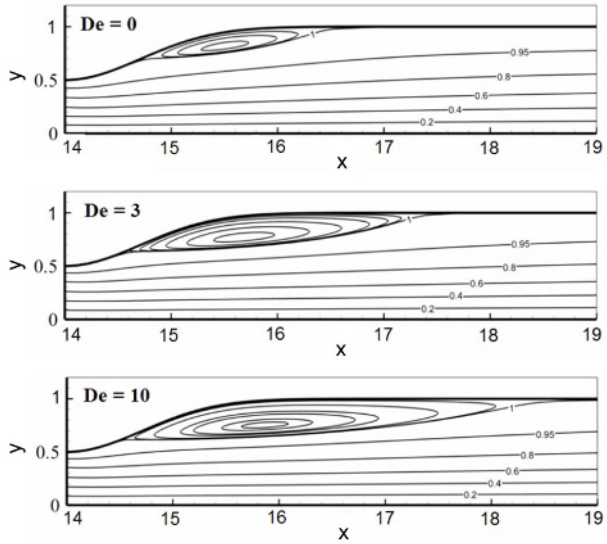

Fig. 21. Effect of the Deborah number, *De*, on the size of the recirculatory zone downstream of throat (Re = 50, ε = 0.4, β = 0.7, and δ = 0.5).

et al. (1993)). Higher Reynolds-number results are also useful in high-throughput microfluidic systems equipped with constricted channels as a passive means for mixing enhancement and/or cell separation (Zhang *et al.*, 2019). With this in mind, we have tried to obtain results at moderate Reynolds numbers typical of such applications. The problem is that it is very demanding for current numerical schemes to obtain converged results when the Deborah and Reynolds numbers are simultaneously large. We have been fortunate enough to obtain converged results for Reynolds number up to 50, which happened to be large enough to cause flow separation - which is deemed to be a useful effect in microfluidic systems if not in physiological systems (Rodd *et al.*, 2005). To increase the likelihood of flow separation, simulations are carried out for a larger blockage ratio of δ = 0.5. Figure 20 presents typical results obtained for Re = 50 at several Deborah numbers. This figure shows that a flow reversal is occurring downstream of the throat which is aggravated by an increase in the Deborah number. No such flow reversal could be detected at Re = 1, and so the results obtained at Re = 50 is a clear manifestation of the importance of inertia effects, as previously noted by Perera and Walters (1977). The prediction that elastic effects give rise to an enlargement of the separated zone (see Fig. 20) is also nothing new and has been previously reported in the literature (Aguayo *et al.*, 2008). The same is true as to the effect of the shear-thinning which has been shown to play a key role in such flows (Fernandes *et al.*, 2019). Obviously, as far as the size of the separated zone is concerned (see Fig. 21), there is a strong competition between elasticity, shear-thinning, and inertia effects all trying to control the vortex structure. For LPTT fluids, the net effect appears to be an enlargement of the vortex size, at least for this set of parameters. The experimental data reported in Rodd *et al.* (2005) for a 5% PEO solution support this prediction although under creeping-flow condition, it is known that the Deborah number reduces the size of the separated zone in sudden-expansion flow (Poole *et al.*, 2009).

Figure 22 shows the effect of Deborah number on the

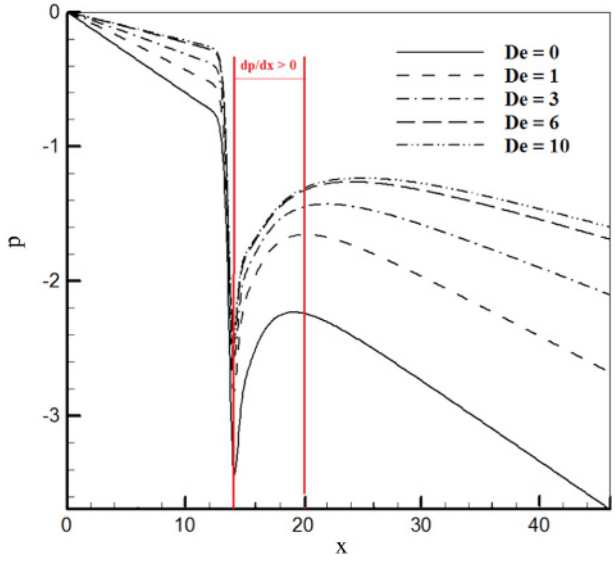

Fig. 22. (Color online) Effect of the Deborah number on the wall pressure variation. The region in which the pressure gradient is positive has been roughly marked (Re = 50, ε = 0.4, β = 0.7, and δ = 0.5).

pressure variation along the channel. The pressure is minimum at the throat which is then increased with its maximum occurring somewhere between $x = 12$ to $x = 16$ depending on the Deborah number. This suggests that there exists a region of positive pressure gradient right after the throat which might be strong enough to cause flow reversal. This figure clearly shows that the region of positive pressure gradient is extended in the x-direction when the Deborah number is increased. It also becomes more severe this way which is why the size of the re-circulatory region is enlarged when the Deborah number is increased.

5. Concluding Remarks

Flow through constricted channels has been proposed in the past as an efficient means for measuring the extensional viscosity of viscoelastic fluids. The technique, however, is based on the premise that for strain-hardening fluids there exists an excess pressure drop as compared with its Newtonian counterpart. Although an excess pressure drop has indeed be recorded for constant-viscosity Boger fluids, for shear-thinning viscoelastic fluids such as LPTT recent numerical results obtained in flow of shear-thinning viscoelastic fluids such as LPTT (through orifice plates) could not record any excess pressure drop. We have relied on the OpenFoam software for simulating the flow of this particular fluid through a cosinusoidal constriction at a typically small Reynolds number of "one" and reached the conclusion that the pressure drop incurred is indeed in excess of the baseline provided that instead of Newtonian baseline use is made of an equivalent power-law baseline. We have also obtained numerical results at Reynolds numbers as high as 50 and found out that a flow reversal might be witnessed at the lee side of the channel even at such a moderate Reynolds numbers inferring that this technique of assessing extensional viscosity cannot be used at large Reynolds numbers due to the limitations posed by the nontrivial end effects. The high-Reynolds-number results, however, might be very useful in high-throughput microfluidic systems where a constriction can be used to enhance mixing through flow separation downstream of the throat. Our numerical results also suggest that in microfluidic application of constrictions the Deborah number should be as large as possible as it lowers the pressure drop induced by the constriction.

Acknowledgment

The authors would like to thank the respectful reviewers for their constructive comments. The support received from Satellite Research Institute (Iranian Space Research Center), under contract number 96/1050/394, is also gratefully acknowledged.

Appendix A: Determining extensional viscosity using pressure-drop data

As mentioned in the main body of the text, in this work we are not directly involved with predicting the extensional viscosity of LPTT fluids using the pressure-drop data. But, for completeness, we briefly describe how *epd* can be used for this purpose. Based on their comprehensive analysis, Nyström *et al.* (2016) proposed the following relationship to correlate *epd* with extensional viscosity:

$$\eta_E(\dot{\varepsilon}) \approx epd \cdot \phi(\dot{\varepsilon})\dot{\varepsilon} \tag{A1}$$

where $\phi(\dot{\varepsilon})$ is called the dissipation function which depends on the fluid under investigation. For example, for

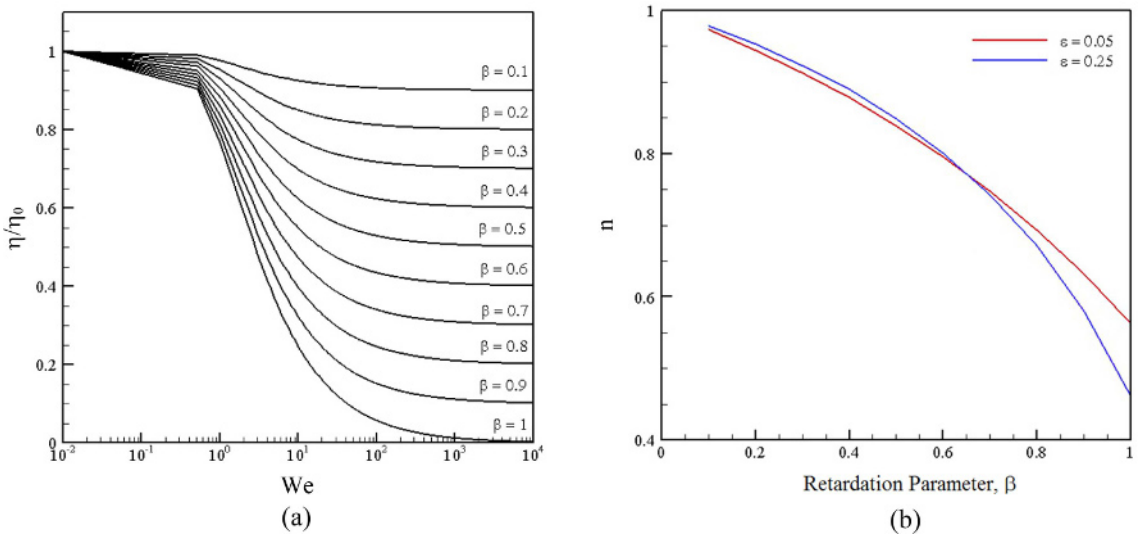

Fig. B1. (Color online) Effect of the viscosity ratio, β, on the shear viscosity profiles of the LPTT fluid ($\varepsilon = 0.25$). The power-law index is obtained through curve-fitting to the viscosity data in the range of $1 < De < 10$.

WM-FENE-CR fluids they proposed the following equation for this function:

$$\eta_E(\dot{\varepsilon}) \approx epd \cdot (1 + (\lambda_D \dot{\varepsilon})^2)\dot{\varepsilon} \tag{A2}$$

where λ_D is the material's diffusion time. Another idea is to correlate the pressure drop due to extension Δp_{ext} with the first normal stress difference in extension, $(\tau_{xx} - \tau_{yy})$ (Cogswell, 1972; James *et al.*, 1990). An apparent extensional viscosity can then be defined as:

$$\eta_E(\dot{\varepsilon}) = \frac{\tau_{xx} - \tau_{yy}}{\dot{\varepsilon}_a} \approx \frac{\Delta p_{ext}}{\dot{\varepsilon}_a} \tag{A3}$$

where $\dot{\varepsilon}_a$ is the apparent rate of extension. On the other hand, we have: $\Delta p_{ext} = (\Delta p - \Delta p_{fd})_{PTT} - (\Delta p - \Delta p_{fd})_{in}$ where the subscript "in" stands for the pressure drop associated with the inelastic analogue of the LPTT fluid, which is obtained by fitting a purely-elastic, shear-thinning model such as power-law to the viscosity profile of the LPTT fluid. To estimate $\dot{\varepsilon}_a$, the axial velocity is estimated as: $u(x) = Q/h(x)$ where the width of the channel has been set equal to 1. In this relationship, $h(x)$ stands for the shape of the constriction, and Q is the flow rate (which can be obtained knowing the Poiseuille-flow velocity profiles at the inlet section of the channel). The extension rate can then be obtained as $\dot{\varepsilon}(x) = du/dx$ which is obviously inhomogeneous for the cosinusoidal profile chosen in this work. An apparent extension rate can be defined as an average between its values at the inlet section of the constriction and that at its throat; that is:

$$\dot{\varepsilon}_a = \frac{\dot{\varepsilon}\big|_{x=L_u} + \dot{\varepsilon}\big|_{x=L_u+0.5}}{2}. \tag{A4}$$

The apparent extensional viscosity obtained this way can be useful for quality control purposes.

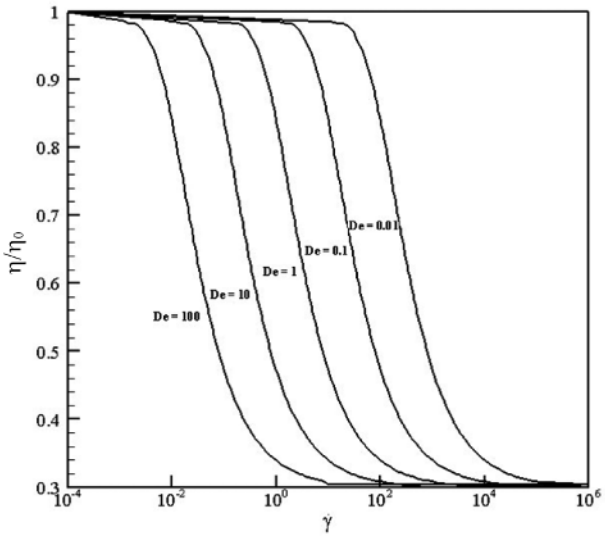

Fig. B2. Effect of the Deborah number (*De*) on the shear viscosity profile of the LPTT model (ε = 0.25).

Appendix B: Power-law index of LPTT fluids

To find the power-law index of LPTT fluids, as the first task, we have to obtain the viscosity profiles for this fluid. The required formulations have already been worked in the literature (Xue *et al.* (1998), Ngamaramvaranggul and Webster (2002), and Oliveira and Pinho (1999)). Figure B1a shows typical viscosity profiles for this fluid at different retardation parameters. In Figure B1b we have also shown the power-law exponent and its variation with the retardation parameters for two different extensional parameters. We have also obtained the viscosity profiles for different Deborah numbers (see Fig. B2), and reached to the conclusion that, the power-law exponent for all of them is roughly 0.75 (*i.e.*, independent of *De*) as long as the Deborah number is between 1 and 10.

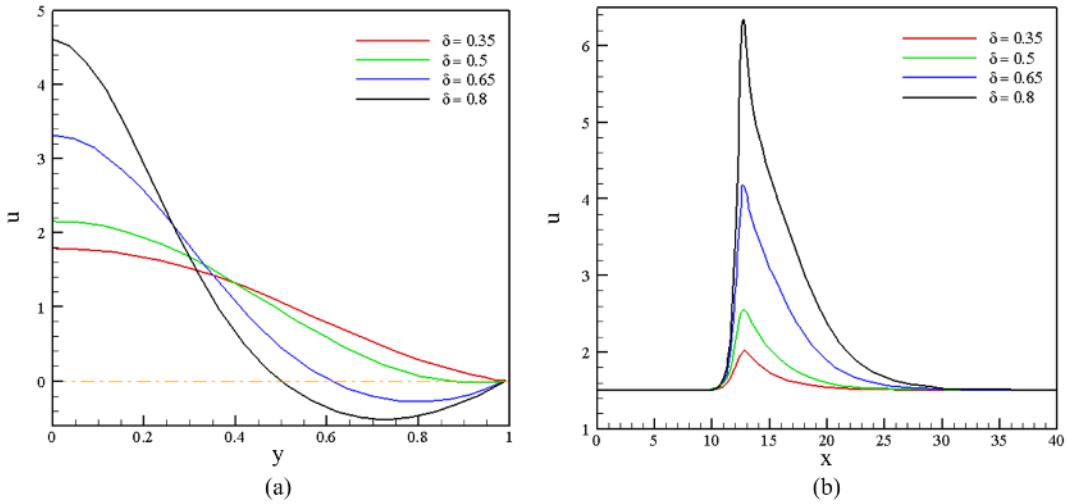

Fig. C1. (Color online) Effect of the stenosis height on the axial velocity profile (*Re* = 70, *De* = 0, ε = 0, and L_c = 1), (a) velocity profile at x = 15 and (b) velocity distribution along the centerline.

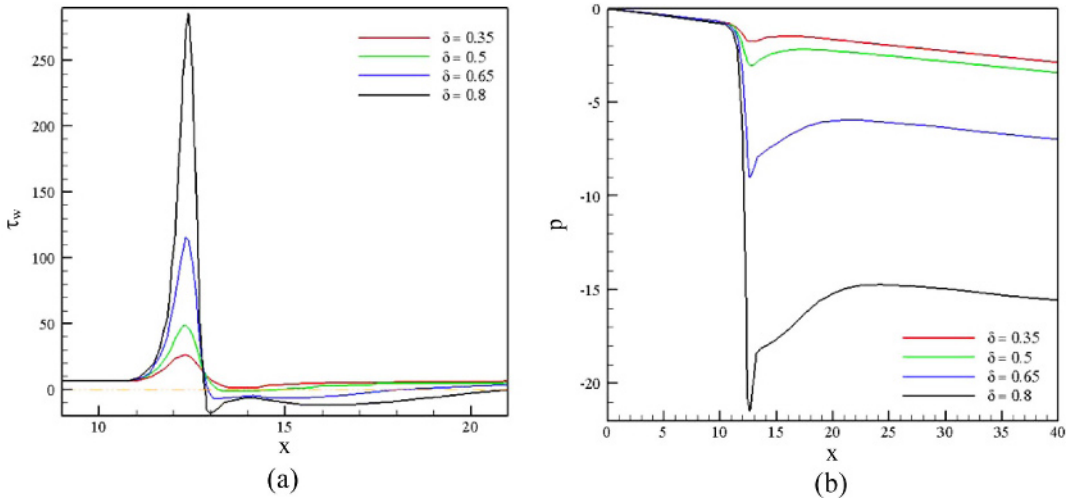

Fig. C2. (Color online) Effect of the stenosis height on flow characteristics (Re = 70, De = 0, ε = 0, and L_c = 1), (a) shear stress variation at the wall and (b) pressure variation along the centerline.

Appendix C: Effect of the geometrical parameters

Flow through constricted channels are frequently encountered in the circulation system of human body where stenosis is realized to be a common problem in aged people. The blockage ratio and the span of the constriction are key parameters which may affect normal blood flow (say, the pressure drop). Thus, it would be a good idea to investigate their effects in this work. The effect of these two parameters has not been investigated by Tammadon-Jahromi *et al.* (2011) - perhaps because their effects looked trivial - and so can be regarded as an extension of their results. Figures C1 and C2 show the role played by the height of the constriction on the flow characteristics for a given set of parameters. The strong effect of "δ" on the flow characteristics is evident in these figures. As can be seen in Fig. C1a, an increase in the height of the constriction may give rise to flow reversal. The velocity at the throat is also dramatically increased when δ increased. The same is true as to its effect on the wall shear stress and pressure drop, *i.e.*, both are an increasing function of the blockage ratio, as expected.

Figures C3 and C4 show the effect the constriction's length (L_c) on the flow characteristics for a given set of parameters (The orifice plate is an extreme case of our constriction where the length of the constriction is very small). Qualitatively, the effect of L_c on the flow characteristics is predicted to be the same as the effect of δ. But, quantitatively, its effect is less significant than δ. Obviously, an increase in L_c diminishes the severity of any adverse effects. For example, the size of the vortex downstream of the constriction shrinks when L_c is increased (see Fig. C1a). On the other hand, the centerline velocity

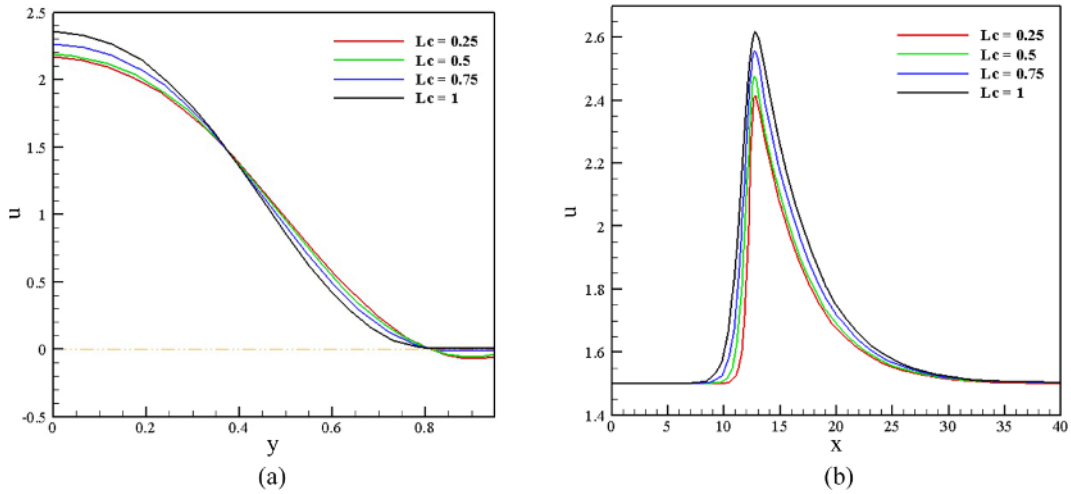

Fig. C3. (Color online) Effect of the stenosis length on the axial velocity profile (Re = 70, De = 0, ε = 0, and δ = 0.5), (a) velocity profile at x = 15 and (b) velocity distribution along the centerline.

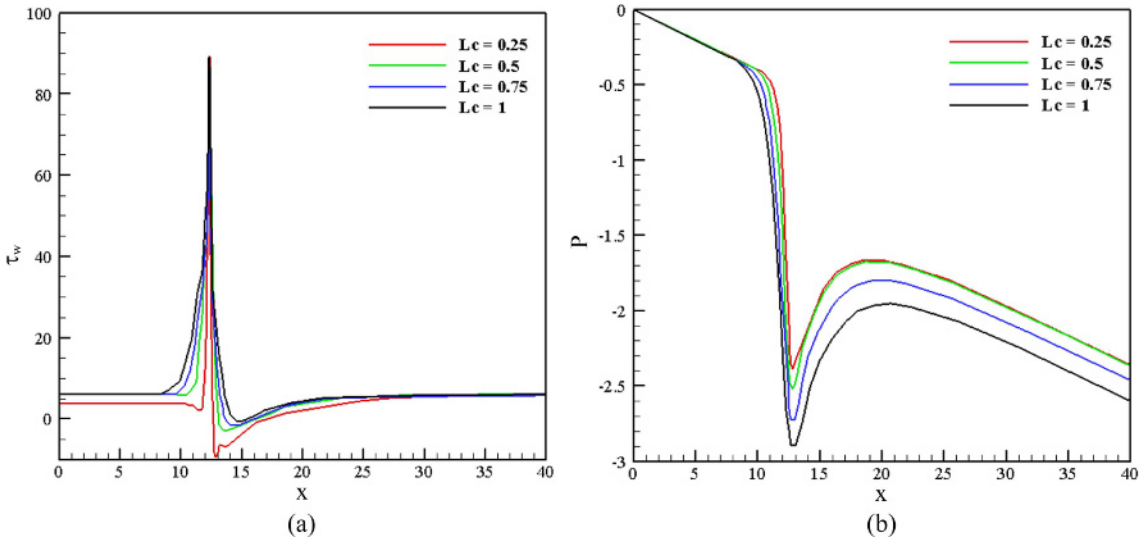

Fig. C4. (Color online) Effect of the stenosis length on the axial velocity profile (Re = 70, De = 0, ε = 0, and δ = 0.5), (a) velocity profile at x = 15 and (b) velocity distribution along the centerline.

is slightly increased (see Fig. C3b). The distribution of the shear stress at the wall becomes smoother the larger the length of the constriction, but, in general, its magnitude is predicted not to be affected that much. The same is true as to its effect on the pressure drop unless the L_c is too extended so that the converging section gives rise to a larger pressure drop (see Fig. C4).

References

Aguayo, J.P., H.R. Tamaddon-Jahromi, and M.F. Webster, 2008, Excess pressure-drop estimation in contraction and expansion flows for constant shear-viscosity, extension strain-hardening fluids, *J. Non-Newton. Fluid Mech.* **153**, 157-176.

Alves, M.A., F.T. Pinho, and P.J. Oliveira, 2001, Study of steady pipe and channel flows of a single-mode Phan-Thien-Tanner fluid, *J. Non-Newton. Fluid Mech.* **101**, 55-76.

Anderson, H.I., R. Halden, and T. Glomsaker, 2000, Effects of surface irregularities on flow resistance in differently shaped arterial stenoses, *J. Biomech.* **33**, 1257-1262.

Azaiez, J., R. Guénette, and A. Ait-Kadi, 1996, Numerical simulation of viscoelastic flows through a planar contraction, *J. Non-Newton. Fluid Mech.* **62**, 253-277.

Binding, D.M., P.M. Phillips, and T.N. Phillips, 2006, Contraction/expansion flows: The pressure drop and related issues, *J. Non-Newton. Fluid Mech.* **137**, 31-38.

Bird, R.B., R.C. Armstrong, and O. Hassager, 1987, *Dynamics of Polymeric Liquids Vol. 1: Fluid Mechanics*, 2nd ed., John Wiley and Sons Inc., New York.

Cheng, R.T.S., 1972, Numerical solution of the Navier-Stokes equations by the finite element method, *Phys. Fluids* **15**, 2098-2105.

Cogswell, F.N., 1972, Converging flow of polymer melts in extrusion dies, *Polym. Eng. Sci.* **12**, 64-73.

Favero, J.L., A.R. Secchi, N.S.M. Cardozo, and H. Jasak, 2010, Viscoelastic flow analysis using the software OpenFOAM and differential constitutive equations, *J. Non-Newton. Fluid Mech.* **165**, 1625-1636.

Fernandes, C., V. Vukčević, T. Uroić, R. Simoes, O.S. Carneiro, H. Jasak, and J.M. Nóbrega, 2019, A coupled finite volume flow solver for the solution of incompressible viscoelastic flows, *J. Non-Newton. Fluid Mech.* **265**, 99-115.

Giddens, D.P., C.K. Zarins, and S. Glagov, 1993, The role of fluid mechanics in the localization and detection of atherosclerosis, *J. Biomech. Eng.* **115**, 588-594.

Grillet, A.M., A.C.B. Bogaerds, G.W.M. Peters, F.P.T. Baaijens, and M. Bulters, 2002, Numerical analysis of flow mark surface defects in injection molding flow, *J. Rheol.* **46**, 651-669.

Harten, A., 1983, High resolution schemes for hyperbolic conservation laws, *J. Comput. Phys.* **49**, 357-393.

James, D.F., 2009, Boger fluids, *Annu. Rev. Fluid Mech.* **41**, 129-142.

James, D.F., G.M. Chandler, and S.J. Armor, 1990, A converging channel rheometer for the measurement of extensional viscosity, *J. Non-Newton. Fluid Mech.* **35**, 421-443.

Larson, R.G., 1988, *Constitutive Equations for Polymer Melts and Solutions*, Butterworths, Boston.

Lee, H.S. and S.J. Muller, 2017, A differential pressure extensional rheometer on a chip with fully developed elongational flow, *J. Rheol.* **61**, 1049-1059.

Lee, J.W., D. Kim, and Y. Kwon, 2002, Mathematical characteristics of the pom-pom model, *Rheol. Acta* **41**, 223-231.

Lopez-Aguilar J.E., M.F. Webster, H.R. Tamaddon-Jahromi, O. Manero, D.M. Binding, and K. Walters, 2017, On the use of continuous spectrum and discrete-mode differential models to predict contraction-flow pressure drops for Boger fluids, *Phys. Fluids* **29**, 121613.

Magda, J.J., J. Lou, S.G. Baek, and K.L. DeVries, 1991, Second normal stress difference of a Boger fluid, *Polymer* **32**, 2000-2009.

Mahapatra, T.R., G.C. Layek, and M.K. Maiti, 2002, Unsteady laminar separated flow through constricted channel, *Int. J. Non-Linear Mech.* **37**, 171-186.

Marrucci, G., F. Greco, and G. Ianniruberto, 2001, Integral and differential constitutive equations for entangled polymers with simple versions of CCR and force balance on entanglements, *Rheol. Acta* **40**, 98-103.

Ngamaramvaranggul, V. and M.F. Webster, 2002, Simulation of pressure-tooling wire-coating flow with Phan-Thien/Tanner models, *Int. J. Numer. Methods Fluids* **38**, 677-710.

Nyström, M., H.R. Tamaddon-Jahromi, M. Stading, and M.F. Webster, 2016, Extracting extensional properties through excess pressure drop estimation in axisymmetric contraction and expansion flows for constant shear viscosity, extension strain-hardening fluids, *Rheol. Acta* **55**, 373-396.

Ober, T.J., S.J. Haward, C.J. Pipe, J. Soulages, and G.H. McKinley, 2013, Microfluidic extensional rheometry using a hyperbolic contraction geometry, *Rheol. Acta* **52**, 529-546.

Oliveira, P.J. and F.T. Pinho, 1999, Analytical solution for fully developed channel and pipe flow of Phan-Thien-Tanner fluids, *J. Fluid Mech.* **387**, 271-280.

Perera, M.G.N. and K. Walters, 1977, Long range memory effects in flows involving abrupt changes in geometry: Part 2: The expansion/contraction/expansion problem, *J. Non-Newton. Fluid Mech.* **2**, 191-204.

Perez-Camacho, M., J.E. Lopez-Aguilar, F. Calderas, O. Manero, and M.F. Webster, 2015, Pressure-drop and kinematics of viscoelastic flow through an axisymmetric contraction-expansion geometry with various contraction-ratios, *J. Non-Newton. Fluid Mech.* **222**, 260-271.

Peters, G.W.M., J.F.M. Schoonen, F.P.T. Baaijens, and H.E.H. Meijer, 1999, On the performance of enhanced constitutive models for polymer melts in a cross-slot flow, *J. Non-Newton. Fluid Mech.* **82**, 387-427.

Phan-Thien, N. and R.I. Tanner, 1977, A new constitutive equation derived from network theory, *J. Non-Newton. Fluid Mech.* **2**, 353-365.

Phan-Thien, N., 1978, A nonlinear network viscoelastic model, *J. Rheol.* **22**, 259-283.

Pimenta, F. and M.A. Alve, 2017, Stabilization of an open-source finite-volume solver for viscoelastic fluid flows, *J. Non-Newton. Fluid Mech.* **239**, 85-104.

Poole, R.J., F.T. Pinho, M.A. Alves, and P.J. Oliveira, 2009, The effect of expansion ratio for creeping expansion flows of UCM fluids, *J. Non-Newton. Fluid Mech.* **163**, 35-44.

Rodd, L.E., D. Lee, K.H. Ahn, and J.J. Cooper-White, 2010, The importance of downstream events in microfluidic viscoelastic entry flows: Consequences of increasing the constriction length, *J. Non-Newton. Fluid Mech.* **165**, 1189-1203.

Rodd, L.E., T.P. Scott, D.V. Boger, J.J. Cooper-White, and G.H. McKinley, 2005, The inertio-elastic planar entry flow of low-viscosity elastic fluids in micro-fabricated geometries, *J. Non-Newton. Fluid Mech.* **129**, 1-22.

Saramito, P., 1995, Efficient simulation of nonlinear viscoelastic fluid flows, *J. Non-Newton. Fluid Mech.* **60**, 199-223.

Sousa, P.C., F.T. Pinho, M.S.N. Oliveira, and M.A. Alves, 2011, Extensional flow of blood analog solutions in microfluidic devices, *Biomicrofluidics* **5**, 014108.

Tamaddon-Jahromi, H.R., I.E. Garduno, J.E. Lopez-Aguilar, and M.F. Webster, 2016, Predicting large experimental excess pressure drops for Boger fluids in contraction-expansion flow, *J. Non-Newton. Fluid Mech.* **230**, 43-67.

Tamaddon-Jahromi, H.R., M.F. Webster, and P.R. Williams, 2011, Excess pressure drop and drag calculations for strain-hardening fluids with mild shear-thinning: Contraction and falling sphere problems, *J. Non-Newton. Fluid Mech.* **166**, 939-950.

Walters, K., H.R. Tamaddon-Jahromi, M.F. Webster, M.F. Tome, and S. McKee, 2009, The competing roles of extensional viscosity and normal stress differences in complex flows of elastic liquids, *Korea-Aust. Rheol. J.* **21**, 225-233.

Wang, J. and D.F. James, 2011, Lubricated extensional flow of viscoelastic fluids in a convergent microchannel, *J. Rheol.* **55**, 1103-1126.

Wapperom, P. and R. Keunings, 2000, Simulation of linear polymer melts in transient complex flow, *J. Non-Newton. Fluid Mech.* **95**, 67-83.

Wapperom, P. and R. Keunings, 2001, Numerical simulation of branched polymer melts in transient complex flow using pom-pom models, *J. Non-Newton. Fluid Mech.* **97**, 267-281.

White, J.L. and A.B. Metzner, 1963, Development of constitutive equations for polymeric melts and solutions, *J. Appl. Polym. Sci.* **7**, 1867-1889.

Xue, S.C., N. Phan-Thien, and R.I. Tanner, 1998, Three dimensional numerical simulations of viscoelastic flows through planar contractions, *J. Non-Newton. Fluid Mech.* **74**, 195-245.

Zhang, Y., Y. Zhao, D. Chen, K. Wang, Y. Wei, Y. Xu, C. Huang, J. Wang, and J. Chen, 2019, Crossing constriction channel-based microfluidic cytometry capable of electrically phenotyping large populations of single cells, *Analyst* **144**, 1008-1015.